Real-time Multi-stability Risk Assessment and Visualization of Power Systems: A Graph Neural Network-based Method

Qifan Chen, *Graduate Student Member, IEEE*, Siqi Bu, *Senior Member, IEEE*, Huaiyuan Wang, and Chao Lei, *Member, IEEE*

***Abstract*—Multi-stability risk assessment (MSRA) is more practical than singular stability risk assessment in power system operation considering increasing uncertainties, e.g., renewable power generation and system faults. In this paper, a real-time MSRA method based on a graph neural network (GNN) is proposed to effectively address multiple stability problems, including (small-disturbance and transient) rotor angle, (short-term and long-term) voltage, frequency, and converter-driven stability. An operating graph and a disturbance graph are developed as input features of GNN to completely characterize complex operating conditions and disturbances. In the GNN, the topology correlations in the inputs can be learned by graph convolutional layers via initial residual identity mapping, resulting in informative high-order features for MSRA. A GraphNorm method is employed in the GNN to tackle over-smoothing problems and improve generalizability effectively. Then, based on real-time data, the risks of the multiple types of stability can be simultaneously and continuously predicted by the GNN, and the stable and unstable operation regions (SURs) can be visualized based on alpha shapes. The effectiveness of the proposed method is verified in the IEEE 39-bus system, the 179-bus western electricity coordinating council (WECC) system, and the Great Britain (GB) system. The comparison results of SURs associated with multi-stability are demonstrated and discussed to prioritize major types of stability problems.**

***Index Terms*—Multi-stability, stability risk, renewable power generation, uncertainty, graph neural network.**

I. Introduction

A. Background

An increasing amount of renewable energy, e.g., wind and solar energy, is integrated into power systems to tackle the climate crisis. As a result, growing uncertainties and decreasing inertia would cause multiple power system stability problems [1]-[3], e.g., (small-disturbance and transient) rotor angle stability, (short-term and long-term) voltage stability, frequency stability, and converter-driven stability according to the updated stability classification in [4], which are named as "multi-stability" for convenience in this paper. Transmission system operators (TSOs) face unprecedented challenges in evaluating the multi-stability risk and improving the security of power system operation with massive uncertainties.

B. Motivation for Multi-stability Risk Assessment (MSRA)

Stability risk assessment (SRA), also called probabilistic stability assessment/analysis [5], [6], is the most widely used stability analysis approach that can assess the effects of uncertainties [5]-[10]. Compared with conventional deterministic stability assessment, SRA can provide not only the probability of different stability margins but also stable and unstable operation regions (SURs) [6], [7]. On this basis, planners and operators can mitigate the stability risks by comprehensively considering the severity and probability of incidents. Hence, the SRA is popular and effective for power systems with high penetration of renewable energy.

The conventional SRA mainly focuses on singular stability [6]-[14]. The effects of various uncertainties, e.g., wind power generation [6], [7], [9], [11], [14], photovoltaic generation [6], [10], loads [12], and plug-in electric vehicles [13], have been considered for the SRA of singular stability, e.g., rotor angle, voltage, frequency, and converter-driven stability. However, the existing studies of singular stability have specific assumptions (e.g., component models) and scenarios. In this case, their study results are fragmented and limited. The impacts of an improvement measure derived based on singular stability may be different or even opposite for other types of stability. By contrast, MSRA aims to study multiple stability problems using the same assumptions and under the same scenario, thereby providing comprehensive analysis results that are all valid for multiple aspects of stability [15], [16]. Actually, different types of stability problems have occurred simultaneously in real power systems. Both frequency instability and short-term voltage instability have been observed in the 2016 South Australia blackout event [1]. In the 2006 Pakistan blackout event, small-disturbance rotor angle instability and short-term voltage instability have been recorded [2]. In these events, the stability risk cannot be completely perceived only based on the SRA of singular stability. In addition, the relationship between different types of stability

This work was supported in part by the National Natural Science Foundation of China for the Research Project under Grant 52077188, and in part by the Hong Kong Research Grant Council for the Research Project under Grants 15208323. (*Corresponding author: Siqi Bu, email: siqi.bu@polyu.edu.hk*)

Qifan Chen and Chao Lei are with Department of Electrical and Electronic Engineering, The Hong Kong Polytechnic University, Kowloon, Hong Kong. (e-mail: qf_chen@foxmail.com; 21118924r@connect.polyu.hk).

Siqi Bu is with Department of Electrical and Electronic Engineering, Shenzhen Research Institute, Research Centre for Grid Modernisation, International Centre of Urban Energy Nexus, Centre for Advances in Reliability and Safety, Research Institute for Smart Energy, and Policy Research Centre for Innovation and Technology, The Hong Kong Polytechnic University, Kowloon, Hong Kong.

Huaiyuan Wang is with the Fujian Key Laboratory of New Energy Generation and Power Conversion, College of Electrical Engineering and Automation, Fuzhou University, Fuzhou 350116, People's Republic of China (e-mail: 79749544@qq.com).

risks (e.g., stable region size/location and priority) is crucial for understanding the multi-stability mechanisms in essence, and hence, is of deep interest to researchers. According to the analysis above, the study of multi-stability risk is in great practical and scientific demands.

C. Motivation for Introducing Graph Neural Network into MSRA

Recently, the multiple stability problems under uncertainties have been addressed by some researchers [15], [16]. In [15], two composite stability indices are proposed to assess the multi-stability, including small-disturbance rotor angle, transient rotor angle, and frequency stability. The composite stability indices curves in a day can be calculated through Monte Carlo simulation (MCS). In [16], considering the uncertainty of renewable energy and loads, the operational boundaries of multi-stability, including small-disturbance and transient rotor angle, long-term voltage, and frequency stability, are established based on MCS. The MSRA in [15] and [16] relies on MCS and time-domain simulation (TDS) / eigenvalue analysis, which is accurate but time-consuming. Conventional solutions to improving the efficiency of SRA include two approaches. One approach is to use analytical methods, e.g., point estimate methods [17], cumulant-based methods [9], and probabilistic collocation methods [10]. However, the accurate analysis results strongly rely on accurate uncertainty modeling and sensitivity terms [5]. The other approach is to use improved MCS-based methods, e.g., Quasi-MCS [13] and Latin hypercube sampling [18]. Compared with the analytical methods, the MCS-based methods are easier to implement and can process scenarios with complex uncertainties. However, the required computational cost is still high [5]. In conventional power systems, planning uncertainty is much higher than operational uncertainty due to the low penetration of renewable energy. In planning duties, it is possible to derive accurate expressions of uncertainty models or provide enough time for MCS and its variants. Hence, the conventional MSRA methods are mainly considered in planning duties. However, it is predicted that the penetration of renewable energy will become even higher [5], resulting in stronger uncertainty of power generation in the short term. In addition, for the sake of system robustness and an increasing requirement of transmission capacity, the topology of a power system will become increasingly complex [19], resulting in stronger uncertainty of faults. Hence, the operational uncertainty will be increasingly strong and cannot be ignored in future power systems. Extremely high assessment efficiency and adaptability to time-varying uncertainty distributions are required by the MSRA of power system operation. The conventional MSRA methods may become inapplicable due to the high computational cost and the difficulty in obtaining accurate expressions of operational uncertainties. Thus, there is an urgent need to find a new method for the MSRA of real-time power system operation with uncertainties.

Emerging deep learning (DL) methods have the advantages of strong fitting ability and high computation speed, which have demonstrated strong power in the SRA of singular stability [20], [21]. The main idea of DL-based SRA is to count the deterministic results of various potential scenarios given by DL methods, thereby calculating the stability risk. Ref. [20] introduces a stacked denoising auto-encoder (SDAE) model for the SRA of transient stability, considering the uncertainty of wind power generation and loads. In [21], a debiased neural network is proposed to predict the cumulative distribution function and probabilistic density function of a transient stability index considering the uncertainty of wind power generation and loads. The existing work verifies that informative and accurate probability of singular stability can be provided by DL methods. Thus, DL methods are considered to have the potential to break out the existing bottleneck of high computational cost in MSRA.

In order to achieve real-time MSRA, massive potential scenarios should be determined in real time by considering the possible values of uncertainties and be assessed by DL methods. Different from conventional real-time pre-fault deterministic stability assessment based on DL [22], the features of the potential scenarios (i.e., steady states) cannot be obtained from a wide-area monitoring system directly. Hence, it is crucial to avoid time-consuming power flow calculation, so that the pre-fault features of the massive potential scenarios can be generated in real time. In existing SRA based on DL, Ref. [21] selects steady state variables, including the active and reactive power of PQ buses and the active power of PV buses, as input features. Ref. [20] supplements the voltage magnitudes of PV buses on the basis of [21]. By assigning the possible values of uncertainties, the features of massive potential scenarios can be generated immediately, and the stability risk can be assessed in real time. Although the above features can be generated directly without power flow calculation, complex scenarios can hardly be represented by these features correctly since topologies and disturbances are also crucial for stability analysis but are seldom considered. Given a group of the features above (i.e., steady states), the stability can be different due to the changes in system topologies and disturbances. Thus, the information of topologies and disturbances also should be considered and be properly represented by the features in the DL-based MSRA.

Graph neural networks (GNNs), as a kind of emerging DL method, can learn non-Euclidean structure data (i.e., graph data) effectively compared with other DL methods, e.g., SDAE [20], recurrent neural networks (RNNs) [23], [24], and convolutional neural networks (CNNs) [25]. Compared with the non-graph features employed in other DL methods, complex topologies and operating conditions can be represented by graph-based features more intuitively and correctly. Compared with conventional DL methods, the topology correlation contained in the graph data can be learned by GNNs effectively, thereby improving the performance of MSRA. In addition, the GNNs have been employed in the field of deterministic stability assessment for singular stability and have demonstrated powerful effects [26]-[30]. Hence, the GNNs are considered to have great application potential in MSRA.

D. Contributions of The Proposed MSRA Method

According to the analysis above, a real-time MSRA method based on GNN is proposed in this paper. The contributions of

this paper are summarized as follows.

1) It is the first time to realize MSRA for real-time duties rather than planning duties concerned by conventional MSRA methods, which can benefit the risk control of system operation with increasing uncertainties. The real-time MSRA is enabled by an emerging GNN, in which graph convolutional layers (GCLs) via initial residual identity mapping and a GraphNorm method are employed to effectively mine topology correlations, tackle over-smoothing problems, and improve generalizability.

2) The risks of multiple types of stability (i.e., rotor angle, voltage, frequency, and converter-driven stability) can be simultaneously and continuously assessed by the proposed method. On this basis, dominant stability problems with high risks can be detected and prioritized in real time, thereby making targeted decisions timely by TSOs. The relationship between the multiple types of stability risks can also be provided to help understand multi-stability mechanisms in essence.

3) The SURs associated with multi-stability can be visualized in real time, which can intuitively reveal the stable operation ranges of uncertainties. Dominant types of instability at potential fault locations can also be visualized in a power network representation, thereby indicating the critical fault locations accurately.

This paper is organized as follows. Section II elaborates on the concept of MSRA and stability indices. Section III introduces the proposed MSRA method. Case study results are shown in Section IV. Conclusions are drawn in Section V.

II. Problem Description

A. Concepts of Multi-stability Probabilistic Assessment

Given a specific operating condition, stability indices may change due to uncertainties in a power system, e.g., wind power generation and system faults. It means that a seemingly secure operating condition may become insecure once the states of uncertainties change. MSRA is to calculate the potential risk of multi-stability (i.e., probabilities and margins) under a given operating condition, which can be regarded as a pre-fault stability assessment. Then, a rule should be provided to guide the optimization of the current operating condition. In this paper, the guidance rule is provided by a commonly used approach [7], [16], [31], i.e., visualizing SURs in a space composed of uncertainties. The SURs can not only indicate stable/unstable regions but also provide how close to the stable/unstable regions and which direction to move.

B. Employed Stability Indices

In this paper, the considered multi-stability includes small-disturbance and transient rotor angle, short-term and long-term voltage, frequency, and converter-driven stability. Different types of stability should be analyzed based on different indices. The small-disturbance rotor angle stability and converter-driven stability can be analyzed together using the same eigenvalue-based index, and hence, are collectively named small-signal stability for convenience in this paper. The voltage stability is further divided into (large-disturbance) short-term and (small-disturbance) long-term voltage stability since they should be analyzed based on different indices. The index of long-term voltage stability can also be calculated using eigenvalue analysis, which is derived from a different matrix compared to the small-signal stability. The short-term and long-term frequency stability can be analyzed using the same index, and thus, are not differentiated and uniformly referred to as frequency stability in this paper. The indices of the different types of stability are briefly listed in TABLE I.

TABLE I
Definition of Stability Margin Levels of Multi-Stability

Stability type	Index	Stability margin level (R_{SSS}, R_{FS}, R_{SVS}, R_{LVS}, R_{TS})	
		2 (Stable)	1 (Unstable)
Small-signal (rotor angle and converter-driven) stability	ζ / %	>0	≤0
Frequency stability	f_{MFD} / Hz	≤0.5	>0.5
Short-term voltage stability	V_R / p.u.	≤0.2	>0.2
Long-term voltage stability	$\lambda_{J,min}$	>0	≤0
Transient (rotor angle) stability	γ / p.u.	>0	≤0

In TABLE I, a larger stability margin level indicates a higher stability margin. For each type of stability, the stability margin level (i.e., R_{SSS}, R_{FS}, R_{SVS}, R_{LVS} and R_{TS}) with value 2 denotes the stable state of this type of stability. The stability margin level with value 1 denotes the unstable state. The stability margin levels are determined by 5 indices ζ, f_{MFD}, V_R, $\lambda_{J,min}$ and γ, respectively, which are calculated as follows.

1) Small-signal (rotor angle and converter-driven) stability

The small-signal stability can be uniformly analyzed by eigenvalue analysis. The index damping ratio ζ can be calculated by

$$\zeta = \frac{-\alpha}{\sqrt{\alpha^2+\omega^2}} \times 100\% , \tag{1}$$

where α and ω are the real and imaginary part of concerned conjugate eigenvalues, which can be derived from a state transition matrix of system. The concerned conjugate eigenvalues can be associated with rotor angle stability and converter-driven stability [13], [32]. Thus, these two types of stability can be analyzed together. The small-signal stability margin level (i.e., R_{SSS}) can be defined according to ζ [13], [32], as shown in TABLE I. When ζ>0%, activated oscillations will decay and the system is stable. Otherwise (i.e., ζ≤0%), activated oscillations will diverge and the system is unstable. In this paper, the minimum ζ is employed to determine R_{SSS}.

2) Frequency stability

The maximum frequency deviation f_{MFD} is the index for frequency stability [7], which can be calculated by

$$f_{MFD} = \max\left(f_{max} - f_s, f_s - f_{min}\right), \tag{2}$$

where f_{max} and f_{min} are the maximum and minimum frequency, respectively, during TDS; and f_s is a nominal frequency. According to [7] and [33], 0.5 Hz can be used as the threshold of f_{MFD} to define the frequency stability margin level (i.e., R_{FS}).

3) Short-term and long-term voltage stability

The short-term voltage stability can be evaluated by the restored voltage level after a large disturbance, which can be indicated by

$$V_R = \max\left(\left|V_{max}-1\right|, \left|V_{min}-1\right|\right), \tag{3}$$

where V_{max} and V_{min} are the maximum and minimum restored bus voltage, respectively, during TDS. A power system can be

regarded as short-term voltage stable once a certain voltage level can be restored. In the existing work, 0.2 p.u. is usually employed as the threshold for V_R to assess the short-term voltage stability [26]. It means that the system is short-term voltage stable if all bus voltage can be restored to the range from 0.80 p.u. to 1.20 p.u. Accordingly, the short-term voltage stability margin level (i.e., R_{SVS}) can be defined in TABLE I.

Different from the short-term voltage stability, the long-term voltage stability can be analyzed based on eigenvalue decomposition of a reduced Jacobian matrix [14]. Given linearized steady-state voltage equations as

$$\begin{bmatrix} \Delta \boldsymbol{P} \\ \Delta \boldsymbol{Q} \end{bmatrix} = \boldsymbol{J} \begin{bmatrix} \Delta \boldsymbol{\theta} \\ \Delta \boldsymbol{U} \end{bmatrix}, \tag{4}$$

where $\Delta \boldsymbol{P}$, $\Delta \boldsymbol{Q}$, $\Delta \boldsymbol{\theta}$, and $\Delta \boldsymbol{U}$ are the variation vectors of bus active, reactive power injection, bus voltage angle, and voltage magnitude, respectively; and $\boldsymbol{J}$ is the reduced Jacobian matrix of concerned buses. The index $\lambda_{J,min}$ is a real number and can be derived by calculating the minimal eigenvalues of $\boldsymbol{J}$. A system is long-term voltage stable if all eigenvalues of $\boldsymbol{J}$ are positive, i.e., $\lambda_{J,min} > 0$. Otherwise, the system is long-term voltage unstable. Then, the long-term voltage stability margin level (i.e., R_{LVS}) can be defined in TABLE I.

4) Transient (rotor angle) stability

The index γ is a widely used index for transient stability [6], [34], [35], which can be calculated by

$$\gamma = \frac{360 - \delta_{max}}{360 + \delta_{max}} \times 100, \tag{5}$$

where δ_{max} is the maximum rotor angle difference between any two generators at the same moment during TDS. A widely used criterion for transient instability is to judge whether $\delta_{max} \geq 360°$, i.e., $\gamma \leq 0$ [6], [34], [35]. Accordingly, the transient stability margin level (i.e., R_{TS}) can be defined in TABLE I.

5) Overall stability

Based on the stability margin levels of the multiple stability above, an overall stability margin level R_{OS} is defined by

$$R_{OS} = \min\left(R_{SSS}, R_{FS}, R_{SVS}, R_{LVS}, R_{TS}\right), \tag{6}$$

where R_{SSS}, R_{FS}, R_{SVS}, R_{LVS} and R_{TS} are the stability margin levels of different types of stability determined according to TABLE I, respectively. The R_{OS} is conservative, which is determined by the lowest stability margin level of multi-stability.

Actually, the stability indices, margin levels, and standards above are employed to demonstrate the effects of the proposed MSRA method. Operators can select the concerned indices, develop suitable standards, and define more stability margin levels based on the practical situations of their grids.

C. Uncertainty Sources

Considering different analysis targets and time scales, different uncertainties should be considered [5]. Two types of uncertainties are considered as examples to demonstrate the proposed MSRA method, including *a)* wind power generation (wind speed) change and *b) N-k* contingencies including three-phase-to-ground fault at critical transmission lines and synchronous generator (SG) trip without faults. It should be pointed out that the uncertainties in a power system are not limited to the above two. In this paper, the above two are selected as representative uncertainties. The proposed method is also available for other types of uncertainty if necessary. By combining the above uncertainties, the following two types of disturbance cases can be generated.

- *Disturbance case 1:* the steady state is changed due to the uncertainty of wind power generation first, and then a three-phase-to-ground fault occurs at a transmission line randomly.
- *Disturbance case 2:* the steady state is changed due to the uncertainty of wind power generation first, and then an SG is tripped randomly.

Both the disturbance cases 1 and 2 consider the superposition of two types of uncertainty. For the above disturbance cases, the margin levels of small-signal stability (i.e., R_{SSS}) and long-term voltage stability (i.e., R_{LVS}) are derived by eigenvalue analysis, respectively, at a steady state. The stability margin levels of frequency, short-term voltage, and transient stability (i.e., R_{FS}, R_{SVS}, and R_{TS}) are derived by TDS.

For power system operation, the distribution of wind power generation in the near future (e.g., 15 minutes) can change in real time, and thus can hardly be described by a specified distribution function widely used in power system planning, such as a Weibull or Gaussian distribution. Fortunately, the distribution of wind power generation in the near future can be easily derived in real time by ultra-short-term nonparametric probabilistic wind power forecasting technologies without assuming specified distributions [36]. The probabilistic distributions of fault lines and tripped SGs can be obtained from historical statistics [5].

The multi-stability under serious faults, e.g., *N-k* contingencies ($k \geq 2$), are less affected by operational uncertainties and usually prevented by pre-set emergency control measures. Thus, these contingencies are not considered in this paper. Actually, the proposed method is available for the *N-k* contingencies ($k \geq 2$) if necessary.

III. Proposed MSRA Method Based on GNN

A. Risk Level Assessment based on Graph Neural Network

Both a steady state and a disturbance condition are crucial for stability results. In this section, two graph representations are proposed to represent various operating conditions of a power system and disturbances caused by different uncertainties. Then, the two graphs are regarded as the inputs of a GNN to predict the margin levels of multi-stability.

1) Operating graph: representation for various operating conditions of a power system

A power system can be described by a graph $\mathcal{G} = (\mathcal{V}, \mathcal{E})$, as shown in Fig. 1 as an example.

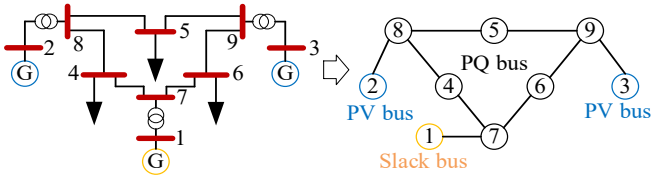

Fig. 1 Graph representation of a power system

In Fig. 1, buses and connection lines can be represented by

nodes and edges, respectively, in the graph. On this basis, the operating condition of the power system can be represented by an operating graph $\mathcal{G}_{\mathrm{OP}}=(\mathcal{V}_{\mathrm{OP}},\mathcal{E}_{\mathrm{OP}})$. $\mathcal{V}_{\mathrm{OP}}\in\mathbb{R}^{N_{\mathrm{B}}\times 4}$ is a matrix of buses. $\mathcal{E}_{\mathrm{OP}}\in\mathbb{R}^{2\times 2N_{\mathrm{L}}}$ is a matrix of connection lines, including the connection relationship between any two buses. $\mathcal{V}_{\mathrm{OP}}$ and $\mathcal{E}_{\mathrm{OP}}$ are defined by

$$\mathcal{V}_{\mathrm{OP}}=\left[\boldsymbol{v}_{\mathrm{OP},1},\cdots,\boldsymbol{v}_{\mathrm{OP},N_{\mathrm{B}}}\right]^{\mathrm{T}}, \tag{7}$$

$$\mathcal{E}_{\mathrm{OP}}=\left[\boldsymbol{e}_{\mathrm{OP},1},\cdots,\boldsymbol{e}_{\mathrm{OP},2N_{\mathrm{L}}}\right], \tag{8}$$

where N_{B} is the number of buses; each bus has 4 features, i.e., $\boldsymbol{v}_{\mathrm{OP},i}=[v_{\mathrm{OP},i,1},\ \ldots,\ v_{\mathrm{OP},i,4}]^{\mathrm{T}}$; N_{L} is the number of connection lines; and $\boldsymbol{e}_{\mathrm{OP},i}=[e_{\mathrm{OP},1,i},\ e_{\mathrm{OP},2,i}]^{\mathrm{T}}$ includes the start bus and end bus of the i-th connection line. Considering the two-way flow of power in a connection line, each connection line is represented by two edges with interchanged bus numbers.

The 4 features include active power, reactive power, voltage magnitude, and voltage angle. The active power and voltage magnitude of a PV bus (i.e., generator), the active power and reactive power of a PQ bus (i.e., load), and the voltage magnitude and angle of a slack bus can be assigned according to a specific scenario. The other features are set as zero.

Based on $\mathcal{E}_{\mathrm{OP}}$, a weighted adjacency matrix $\boldsymbol{A}_{\mathrm{OP}}\in\mathbb{R}^{N_{\mathrm{B}}\times N_{\mathrm{B}}}$ is derived to describe the connections between buses, where an element $a_{\mathrm{OP},i,j}$ at the i-th row and j-th column is derived by

$$a_{\mathrm{OP},i,j}=\begin{cases}\left|z_{i,j}\right|, & \text{if } [i,j]^{\mathrm{T}}\in\{\boldsymbol{e}_{\mathrm{OP},1},\cdots,\boldsymbol{e}_{\mathrm{OP},2N_{\mathrm{L}}}\}\\ 0, & \text{otherwise}\end{cases}, \tag{9}$$

where $z_{i,j}$ is the admittance of the transmission line or transformer connecting the i-th and the j-th buses; a non-zero value of $a_{\mathrm{OP},i,j}$ indicates a connection between two buses; and a zero value indicates a disconnection. The weighted adjacency matrix $\boldsymbol{A}_{\mathrm{OP}}$ is similar to the concept of a branch admittance matrix in power system theories.

Based on $\mathcal{G}_{\mathrm{OP}}=(\mathcal{V}_{\mathrm{OP}},\mathcal{E}_{\mathrm{OP}})$ and $\boldsymbol{A}_{\mathrm{OP}}$, operating conditions with different topologies can be represented as follows.

- When the transmission line connecting the i-th and the j-th buses is disconnected,

$$a_{\mathrm{OP},i,j}=0 \ \text{ and } \ a_{\mathrm{OP},j,i}=0\,. \tag{10}$$

- When the i-th bus is disconnected,

$$\begin{cases}\boldsymbol{v}_{\mathrm{OP},i}=\boldsymbol{0}\\ a_{\mathrm{OP},i,j}=0 \text{ and } a_{\mathrm{OP},j,i}=0,\ j=1,2,\cdots,N_{\mathrm{B}}\end{cases}. \tag{11}$$

The time consumption of a large amount of power flow calculation can hardly be ignored by real-time MSRA. According to the principle of power flow calculation, operating conditions cannot be reflected by $\mathcal{V}_{\mathrm{OP}}$ only, which is employed as input features by traditional neural networks like [20] and [21]. In the proposed method, the operating conditions can be accurately reflected by the graph $\mathcal{G}_{\mathrm{OP}}$ due to the supplemental topology information in $\boldsymbol{A}_{\mathrm{OP}}$. In addition, power flow calculation can be avoided to generate the input features $\mathcal{G}_{\mathrm{OP}}$ and $\boldsymbol{A}_{\mathrm{OP}}$, thereby accelerating the assessment speed of MSRA.

2) Disturbance graph: representation for disturbances due to different uncertainties

Similar to the operating graph defined above, a disturbance graph $\mathcal{G}_{\mathrm{D}}=(\mathcal{V}_{\mathrm{D}},\mathcal{E}_{\mathrm{D}})$ and a corresponding weighted adjacency matrix $\boldsymbol{A}_{\mathrm{D}}$ can be defined. Various disturbances induced by different uncertainties can be represented as follows.

- When a three-phase-to-ground short circuit fault occurs at the line connecting the i-th and j-th buses and then the line is cut off,

$$a_{\mathrm{D},i,j}=\alpha_{\mathrm{F}}\left|z_{i,j}\right| \ \text{ and } \ a_{\mathrm{D},j,i}=\alpha_{\mathrm{F}}\left|z_{i,j}\right|, \tag{12}$$

where α_{F}=0. The other types of faults, e.g., single-phase-to-ground short circuit fault and double-phase-to-ground short circuit fault, can be easily represented by defining a different α_{F}, e.g., 2/3 and 1/3, respectively.

- When a generator at the i-th bus trips,

$$\begin{cases}\boldsymbol{v}_{\mathrm{D},i}=\boldsymbol{0}\\ a_{\mathrm{D},i,j}=0 \text{ and } a_{\mathrm{D},j,i}=0,\ j=1,2,\cdots,N_{\mathrm{B}}\end{cases}. \tag{13}$$

- When the output power of a generator or the consumed power of a load at the i-th bus increases/decreases by $\Delta\boldsymbol{v}_{\mathrm{D}}$,

$$\boldsymbol{v}_{\mathrm{D},i}=\boldsymbol{v}_{\mathrm{OP},i}\pm\Delta\boldsymbol{v}_{\mathrm{D}}\,. \tag{14}$$

As for the other elements in $\mathcal{G}_{\mathrm{D}}$, they are the same as the corresponding elements in $\mathcal{G}_{\mathrm{OP}}$. Then, $\mathcal{G}_{\mathrm{D}}$ and $\boldsymbol{A}_{\mathrm{D}}$, together with $\mathcal{G}_{\mathrm{OP}}$ and $\boldsymbol{A}_{\mathrm{OP}}$, are used as the input of the proposed GNN.

It should be noted that, if necessary, N-k ($k\geq 2$) contingencies can also be represented by setting multiple disturbances in $\mathcal{G}_{\mathrm{D}}$.

3) Proposed graph neural network

A GNN has the ability to learn from non-Euclidean data $\mathcal{G}_{\mathrm{OP}}$ and $\mathcal{G}_{\mathrm{D}}$. The structure of the proposed GNN is shown in Fig. 2.

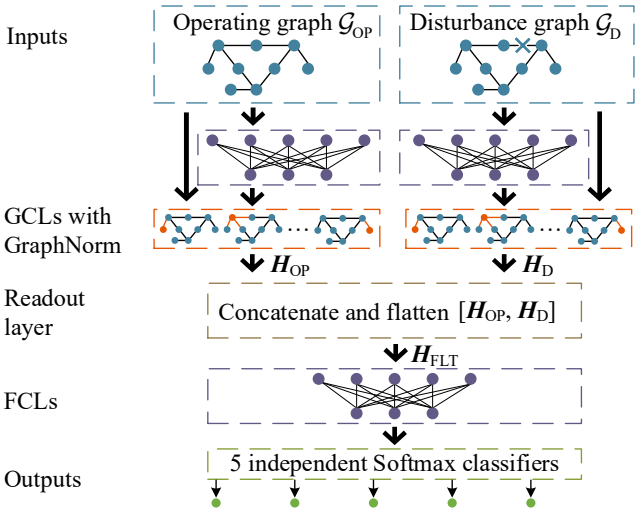

Fig. 2 Structure of proposed GNN

Two independent channels of GCLs are deliberately designed to extract the non-Euclidean structure information of two graphs (i.e., an operating graph $\mathcal{G}_{\mathrm{OP}}$ and a disturbance graph $\mathcal{G}_{\mathrm{D}}$). The operating graph $\mathcal{G}_{\mathrm{OP}}$ with $\boldsymbol{A}_{\mathrm{OP}}$ and the disturbance graph $\mathcal{G}_{\mathrm{D}}$ with $\boldsymbol{A}_{\mathrm{D}}$ are the input features and then are extracted by the two channels, separately. Each channel includes a fully-connected layer (FCL) and multiple GCLs with GraphNorm. The calculation process in each channel is given as follows.

In each channel, the input graph is processed by an FCL by

$$\bar{\boldsymbol{H}}^{(k)}=\mathrm{ReLU}\left(\bar{\boldsymbol{H}}^{(k-1)}\bar{\boldsymbol{W}}^{(k)}+\bar{\boldsymbol{B}}^{(k)}\right), \tag{15}$$

where $\bar{\boldsymbol{H}}^{(k-1)}\in\mathbb{R}^{N_{\mathrm{B}}\times\bar{M}^{(k-1)}}$ is an input matrix; $\bar{\boldsymbol{H}}^{(0)}$ is $\mathcal{V}_{\mathrm{OP}}$ or $\mathcal{V}_{\mathrm{D}}$; $\bar{\boldsymbol{W}}^{(k)}\in\mathbb{R}^{\bar{M}^{(k-1)}\times\bar{M}^{(k)}}$, $\bar{\boldsymbol{B}}^{(k)}\in\mathbb{R}^{N_{\mathrm{B}}\times\bar{M}^{(k)}}$, and $\bar{M}^{(k)}$ are the

weight matrix, bias vector, and set neuron number of the k-th FCL, respectively; and ReLU$(\cdot)$ is a rectified linear unit. In this part, one FCL is employed.

Then, $\bar{\boldsymbol{H}}^{(1)} \in \mathbb{R}^{N_\mathrm{B}\times\bar{M}^{(1)}}$ is input into the following GCLs. Given the input matrix of the k-th GCL $\boldsymbol{H}^{(k-1)} \in \mathbb{R}^{N_\mathrm{B}\times\bar{M}^{(1)}}$ and a weighted adjacency matrix $\boldsymbol{A} \in \mathbb{R}^{N_\mathrm{B}\times N_\mathrm{B}}$, the output of the k-th GCL with normalization can be calculated by

$$\boldsymbol{H}^{(k)} = \mathrm{ReLU}\left(f_{\mathrm{GN}}\left(\begin{pmatrix} \left(\left(1-\alpha^{(k)}\right)\hat{\boldsymbol{P}}\boldsymbol{H}^{(k-1)} + \alpha^{(k)}\boldsymbol{H}^{(0)}\right)\cdot \\ \left(\left(1-\beta^{(k)}\right)\boldsymbol{I} + \beta^{(k)}\boldsymbol{W}^{(k)}\right) \end{pmatrix} \right) \right), \tag{16}$$

$$\hat{\boldsymbol{P}} = \hat{\boldsymbol{D}}^{-1/2}\hat{\boldsymbol{A}}\hat{\boldsymbol{D}}^{-1/2}, \tag{17}$$

where $\hat{\boldsymbol{P}} \in \mathbb{R}^{N_\mathrm{B}\times N_\mathrm{B}}$ is a graph convolution matrix with a renormalization trick; $\boldsymbol{A}$=$\boldsymbol{A}_{\mathrm{OP}}$ or $\boldsymbol{A}_{\mathrm{D}}$; $\hat{\boldsymbol{A}} = \boldsymbol{A} + \boldsymbol{I} = [a_{i,j}]$ and $\boldsymbol{I}$ is an identity matrix; $\hat{\boldsymbol{D}} \in \mathbb{R}^{N_\mathrm{B}\times N_\mathrm{B}}$ is a diagonal matrix and the i-th diagonal element $d_{i,i} = \sum_j a_{i,j}$; $\boldsymbol{W}^{(k)} \in \mathbb{R}^{\bar{M}^{(1)}\times\bar{M}^{(1)}}$ is the weight matrix of the k-th GCL; $\alpha^{(k)}$ and $\beta^{(k)}$ are two hyperparameters; and $\boldsymbol{H}^{(0)} = \bar{\boldsymbol{H}}^{(1)}$, which is the input of the first GCL. The employed GCL uses initial residual identity mapping proposed in [37]. An over-smoothing problem can be prevented, and better performance can be achieved by the employed GCL compared with other variants of GNNs. In addition, a graph normalization technique $f_{\mathrm{GN}}(\cdot)$ is introduced into the GCL, named GraphNorm [38], which is defined by

$$f_{\mathrm{GN}}\left(x_{i,j}\right) = \frac{x_{i,j} - \rho_j \mathbb{E}\left(\boldsymbol{x}_j\right)}{\sqrt{\mathbb{E}\left(\left(x_{i,j} - \rho_j \mathbb{E}\left(\boldsymbol{x}_j\right)\right)^2\right)}}\kappa_j + \eta_j, \tag{18}$$

where $x_{i,j}$ is the element at the i-th row and j-th column in a matrix; $\boldsymbol{x}_j$ is the vector of the j-th column in a matrix; ρ_j is a learnable parameter that decides the information to be retained in the mean; κ_j and η_j are affine parameters; and $\mathbb{E}(\cdot)$ denotes an expected value. Compared with other normalization methods, e.g., BatchNorm, LayerNorm, and InstanceNorm, the employed GraphNorm can make the proposed GNN converge faster and achieve better generalization performance [38].

Then, the outputs of the final GCLs in the two channels (i.e., $\boldsymbol{H}_{\mathrm{OP}}$ and $\boldsymbol{H}_{\mathrm{D}}$) are input into a readout layer by

$$\boldsymbol{H}_{\mathrm{FLT}} = f_{\mathrm{FLT}}\left(\left[\boldsymbol{H}_{\mathrm{OP}}, \boldsymbol{H}_{\mathrm{D}}\right]\right), \tag{19}$$

where $f_{\mathrm{FLT}}(\cdot)$ denotes flattening a matrix into a 1-dimensional vector. The spatial correlation of the input graphs can be captured into the flattened vector $\boldsymbol{H}_{\mathrm{FLT}} \in \mathbb{R}^{1\times 2N_\mathrm{B}\cdot\bar{M}^{(1)}}$ by the GCLs. Then, $\boldsymbol{H}_{\mathrm{FLT}}$ is input into multiple FCLs for the further feature extraction of both operating and disturbance information, which can also be calculated according to (14).

Finally, the output of the final FCL (i.e., the K-th layer) is input into 5 SoftMax classifiers simultaneously to predict the stability margin levels of the concerned multi-stability, respectively. The output vector of the i-th SoftMax classifier can be derived as $\bar{\boldsymbol{Y}}_{\boldsymbol{i}} = \left[\bar{y}_{i,1}, \bar{y}_{i,2}, \cdots, \bar{y}_{i,N_{i,\mathrm{R}}}\right] \in \mathbb{R}^{1\times N_{i,\mathrm{R}}}$. $N_{i,\mathrm{R}}$ is the number of the defined stability margin level of the i-th type of stability, which is 2 in this paper. Then, the stability margin level of i-th type of stability, i.e., R_i, can be judged by

$$R_i = \arg\max_j \left(\bar{y}_{i,j}\right). \tag{20}$$

The R_i derived from the 5 SoftMax classifiers are the predicted R_{SSS}, R_{FS}, R_{SVS}, R_{LVS} and R_{TS}, respectively, and can be substituted into (5) to calculate the overall margin level R_{OS}.

Based on the structure above, the Adam algorithm [39] is utilized to optimize the parameters of the proposed GNN by

$$\boldsymbol{\theta}^* = \arg\min_{\theta}\left(\frac{1}{5N_{\mathrm{train}}}\sum_{l=1}^{N_{\mathrm{train}}}\sum_{i=1}^{5}\sum_{j=1}^{N_{i,\mathrm{R}}} y_{i,j}^{(l)}\log\bar{y}_{i,j}^{(l)}\right), \tag{21}$$

where $\boldsymbol{\theta}^*$ is the optimal parameters of the GNN; N_{train} is the number of training samples; the superscript (l) denotes the l-th sample; and $y_{i,j}^{(l)}$ is the j-th element of a true label vector $\boldsymbol{Y}_i^{(\boldsymbol{l})} \in \mathbb{R}^{1\times N_{i,\mathrm{R}}}$. $y_{i,j}^{(l)}$ is 1 if the margin level of the i-th type of stability is j and otherwise is 0. Based on (20), a well-trained proposed GNN can be obtained when a set training epoch is reached.

B. Visualization of SURs based on Alpha Shapes

In the online application stage of the proposed MSRA method, massive samples (i.e., potential scenarios) are obtained by sampling for uncertainties. Given the input features of such N_{test} samples, i.e., $\{\boldsymbol{X}_{\mathrm{test}}^{(l)}\}$, the proposed GNN can predict the stability margin levels of multi-stability for each sample, i.e., $\{\boldsymbol{R}^{(l)}\}$=$\{[R_{\mathrm{SSS}}, R_{\mathrm{FS}}, R_{\mathrm{SVS}}, R_{\mathrm{LVS}}, R_{\mathrm{TS}}, R_{\mathrm{OS}}]^{(l)}\}$. By selecting concerned features $\boldsymbol{X}_{\mathrm{v}}$ from $\boldsymbol{X}_{\mathrm{test}}$ as axes, each sample can be represented as a point in the space consisting of $\boldsymbol{X}_{\mathrm{v}}$. In [7], convex hulls are employed to generate operation regions of frequency stability effectively. Considering the nonlinear characteristics of power systems, alpha shapes [40], which can be non-convex, are more suitable for generating the SURs of multi-stability.

In this paper, naive SURs are defined as the SURs considering a single fault. By selecting N_{sel} samples with the same fault (e.g., the same fault line) from the set $\{\boldsymbol{X}_{\mathrm{test}}^{(l)}, \boldsymbol{R}^{(l)}\}$, naive SURs can be generated by *Algorithm 1*.

Algorithm 1: Naive SURs generation based on alpha shapes

Input: Concerned features $\{\boldsymbol{X}_{\mathrm{v}}^{(l)}\}$ and predicted stability margin levels $\{r^{(l)}\}$ of N_{sel} selected samples
Output: Naive SURs $\{\boldsymbol{S}_{\alpha,\mathrm{s}}, \boldsymbol{S}_{\alpha,\mathrm{u}}\}$
1: For j=1:2 do
2: Generate set $\boldsymbol{\Omega}_{\alpha,j}$=$\{\boldsymbol{X}_{\mathrm{v}}^{(l)}\}$, where l satisfies $r^{(l)}$=j;
3: Generate unstable region based on alpha shape $\boldsymbol{S}_{\alpha,\mathrm{u}}$ for points in $\boldsymbol{\Omega}_{\alpha,1}$;
4: Generate stable region based on alpha shape $\boldsymbol{S}_{\alpha,\mathrm{s}}$ for points in $\boldsymbol{\Omega}_{\alpha,2}$;
5: End

In *Algorithm 1*, the generation of alpha shapes can refer to [40]. The input r can be R_{SSS}, R_{FS}, R_{SVS}, R_{LVS}, R_{TS}, or R_{OS} to form the naive SURs associated with the corresponding type of stability.

Integrated SURs are defined as the SURs considering multiple faults. Considering N_{f} types of faults (e.g., different fault lines), N_{f} groups of naive SURs can be generated and further integrated as integrated SURs by *Algorithm 2*.

Algorithm 2: Integrated SURs generation based on alpha shapes

Input: N_{f} groups of naive SURs $\{\boldsymbol{S}_{\alpha,\mathrm{s}}^{(n)}, \boldsymbol{S}_{\alpha,\mathrm{u}}^{(n)}\}$, where n=1, 2, … , N_{f}
Output: Integrated SURs $\{\boldsymbol{S}_{A,\mathrm{s}}, \boldsymbol{S}_{A,\mathrm{u}}\}$
1: Define alpha shapes of empty SURs $\{\boldsymbol{S}_{A,\mathrm{s}}, \boldsymbol{S}_{A,\mathrm{u}}\}$;
2: For n=1:N_{f} do
3: Add $\boldsymbol{S}_{\alpha,\mathrm{u}}^{(n)}$ into unstable regions $\boldsymbol{S}_{A,\mathrm{u}}$; and add $\boldsymbol{S}_{\alpha,\mathrm{s}}^{(n)}$ into $\boldsymbol{S}_{A,\mathrm{s}}$;
4: Delete the points of $\boldsymbol{S}_{A,\mathrm{s}}$ that are in $\boldsymbol{S}_{A,\mathrm{u}}$;
5: Reconstruct alpha shapes of the remaining points of $\boldsymbol{S}_{A,\mathrm{s}}$ as stable regions;
6: End

Based on *Algorithm 2*, the naive SURs of minor faults with small unstable regions can be integrated to control their risks

uniformly. As for serious faults with large unstable regions, targeted control measures should be determined. In addition, the dominant types of instability can be determined according to the naive/integrated SURs associated with multi-stability. Furthermore, the critical fault locations can be easily visualized in a power network representation according to the naive/integrated SURs of each potential fault. The types, degrees, and locations of multi-stability risks can be comprehensively and intuitively understood by operators according to the visualized results, and hence, the most effective control measures can be determined.

It should be noted that uniform sampling is employed to generate samples for SURs visualization so that all uncertainty space can be covered. If there are more than three uncertainties concerned as axes, some of the uncertainties can be fixed as constant values (e.g., the maximum and minimum) one by one to visualize the SURs. Alternatively, the values of several uncertainties (e.g., wind power generation) can be aggregated as one variable, like [16].

C. Procedure of Proposed MSRA Method

The procedure of the proposed MSRA method is illustrated in Fig. 3. The procedure can be divided into offline training, online application, and offline update stages.

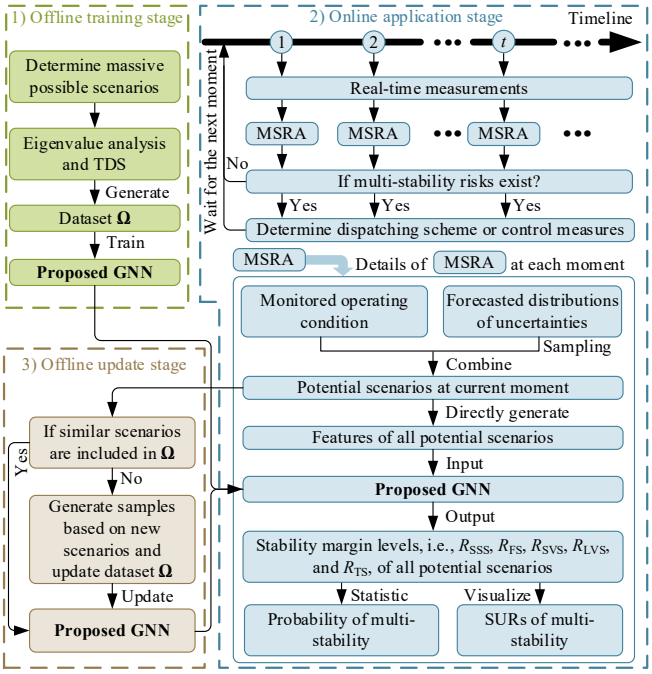

Fig. 3 Procedure of proposed MSRA method

1) Offline training stage

In the offline training stage, massive possible scenarios can be determined according to the comprehensive consideration of operational plans, historical records, and concerned uncertainties (e.g., disturbance cases 1 and 2 in this paper). Eigenvalue analysis and TDS are utilized to derive the stability margin levels of multi-stability (i.e., R_{SSS}, R_{FS}, R_{SVS}, R_{LVS} and R_{TS}) for each scenario. Then, a training dataset $\boldsymbol{\Omega}=\{\boldsymbol{X}_{train}, \boldsymbol{Y}_{train}\}$ can be established, where $\boldsymbol{X}_{train}$ and $\boldsymbol{Y}_{train}$ are the features and labels of training samples, respectively. $\boldsymbol{X}_{train}$ consists of an operating graph $\mathcal{G}_{OP}$ and a disturbance graph $\mathcal{G}_{D}$. $\boldsymbol{Y}_{train}$ includes the values of R_{SSS}, R_{FS}, R_{SVS}, R_{LVS} and R_{TS}. Finally, the dataset $\boldsymbol{\Omega}$ can be employed to train the proposed GNN.

2) Online application stage

After the proposed GNN is well-trained offline, an online application stage starts. In the online application stage, the current operating condition can be monitored in real time based on partially installed phasor measurement units (PMUs), i.e., PMUs at the buses of generators and loads. In addition, the distributions of concerned uncertainties (e.g., wind power generation and faults in this paper) can be generated in real time by ultra-short-term nonparametric probabilistic forecasting [36].

On the basis above, the MSRA can be implemented moment by moment as follows. At the current moment, a group of uncertainty values can be obtained by sampling for the latest generated distributions. Massive potential scenarios at the current moment can be obtained by combining the sampled uncertainty values and the monitored operating condition. The features of each scenario, i.e., $\{\boldsymbol{X}_{test}\}$, including the steady states of partial buses (i.e., active power and voltage magnitude of generators, active and reactive power of loads, and voltage magnitude and phase of slack buses), topology, and uncertainty values, can be directly assigned without power flow calculation. The features $\{\boldsymbol{X}_{test}\}$ are input into the proposed GNN immediately to predict the stability margin levels of multi-stability for all the potential scenarios. The probability of multi-stability is calculated by

$$P_{R,i}=\frac{N_{R,i}}{N_{test}}\times 100\%\,, \tag{22}$$

where $P_{R,i}$ is the probability of the index R (e.g., R_{SSS}, R_{FS}, R_{SVS}, R_{LVS}, R_{TS}, and R_{OS}) with value i (e.g., 1 and 2); $N_{R,i}$ is the number of samples with index R of i; and N_{test} is the number of all samples.

In addition to the probability of multi-stability, the SURs associated with multi-stability and critical fault locations can be visualized, respectively, as introduced in Section III.B.

Based on the given probability of multi-stability and visualized results, TSOs can comprehensively understand the potential multi-stability risk of the current operating condition. If there is no risk, TSOs can wait for the next moment and monitor the multi-stability risk continuously. Otherwise, a dispatching scheme or control measures can be determined to mitigate the multi-stability risk accordingly.

3) Offline update stage

Once massive potential scenarios are sampled in the online application stage, the sampled scenarios can be compared with the scenarios in $\boldsymbol{\Omega}$. If the sampled scenarios or their similar scenarios are not learned by the proposed GNN (e.g., topology changes significantly and new contingencies occur), new training samples should be generated based on these sampled scenarios. Then, the proposed GNN can be updated with the new training samples offline.

It should be noted that the update strategy is not the main focus of this paper. Actually, the proposed MSRA method can be combined with other effective update strategies, e.g., transfer learning [28], [41]-[43] and incremental learning [44], to adapt to unseen topologies and contingencies.

IV. Case Study

In order to verify the effectiveness of the proposed MSRA method, three different-scale power systems, i.e., a modified IEEE 39-bus power system, a modified 179-bus western electricity coordinating council (WECC) power system, and a modified Great Britain (GB) power system, are employed as test systems. The system modeling and TDS are conducted based on the tool ANDES [45].

A. Test in A Modified IEEE 39-bus Power System

1) System description

In Fig. 4, the original SGs at buses 35, 37, and 38 are replaced by type-3 wind farms (WFs) (i.e., WF1, 2, and 3), respectively. An additional WF with large capacity is connected to bus 40, i.e., WF4. The maximum active power of WF1, WF2, WF3, and WF4 are 4.0, 4.0, 4.0, and 10.0 p.u., respectively. The power outputs of WF1, WF2, and WF3 are regarded as uncertainties. In practice, the uncertainty distributions of wind power generation can be obtained and updated in real time by nonparametric probabilistic wind power forecasting technologies. In this part, the distribution is forecasted based on a group of virtual wind power data to demonstrate the proposed MSRA method.

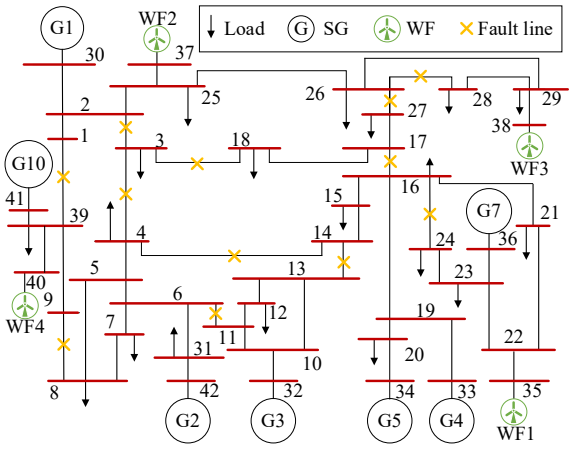

Fig. 4 Line diagram of a modified IEEE 39-bus power system with 4 WFs

As shown in Fig. 4, 12 transmission lines and 6 SGs are considered as potential fault lines and fault SGs, respectively. The probability of fault occurrence is given in TABLE II.

TABLE II
Probability of Fault Occurrence in IEEE 39-bus System

Line bus	Probability	Line bus	Probability	SG	Probability
2-3	7.04%	13-14	3.21%	G1	2.28%
3-4	6.40%	16-17	2.57%	G2	4.55%
3-18	5.77%	16-24	1.93%	G3	6.82%
4-14	5.13%	26-27	0.64%	G4	9.09%
6-11	4.49%	26-28	1.28%	G5	11.36%
8-9	3.85%	39-1	7.69%	G7	15.90%

The probability in TABLE II is set arbitrarily, which does not affect the verification of the proposed method. At system loading levels of 90%, 95%, 100%, 105%, and 110%, considering the disturbance cases 1 and 2, 9832 samples are generated as a training dataset to train a GNN model offline. It should be noted that more types of uncertainties can be considered in practice, and the proposed method is still capable. In this paper, the application procedure of the proposed method is demonstrated by taking the uncertainties above as examples.

2) MSRA based on proposed GNN

The proposed GNN includes two channels and a followed FCL. Each channel has an FCL and two GCLs with GraphNorm. The $\bar{M}^{(k)}$ of the FCL in each channel and the followed FCL are 8 and 128, respectively; For the GCLs, $\alpha^{(1)}$ and $\alpha^{(2)}$ are both 0.1; $\beta^{(1)}$ and $\beta^{(2)}$ are both 0.5; the learning rate of the Adam algorithm is 0.001; and the maximum training epoch is 500.

The proposed method is tested in the following operating condition to verify the performance of online application. The actual system loading level is 98%, which is not included in the training dataset. By randomly sampling from the uncertainties considered in Section IV.A.1), 10000 test samples are generated based on the current operating condition, indicating the potential scenarios induced by the concerned uncertainties. The probability of multi-stability given by the proposed GNN is compared with that given by eigenvalue analysis and TDS, as shown in TABLE III.

TABLE III
Probability of Multi-stability Given by Proposed GNN in IEEE 39-bus System

Method	Margin level i	$P_{R_{\mathrm{SSS},i}}$	$P_{R_{\mathrm{FS},i}}$	$P_{R_{\mathrm{SVS},i}}$	$P_{R_{\mathrm{LVS},i}}$	$P_{R_{\mathrm{TS},i}}$	$P_{R_{\mathrm{OS},i}}$
Proposed GNN	2 (Stable)	89.82%	91.28%	92.79%	100%	98.32%	79.41%
	1 (Unstable)	10.18%	8.72%	7.21%	0%	1.68%	20.59%
Eigenvalue and TDS	2 (Stable)	89.11%	91.23%	93.03%	100%	98.23%	78.76%
	1 (Unstable)	10.89%	8.77%	6.97%	0%	1.77%	21.24%

According to TABLE III, the proposed GNN can predict the accurate probabilities of different types of stability and different stability margin levels, which are quite close to the results given by the time-consuming eigenvalue analysis and TDS. For the probability of transient instability, i.e., $P_{R_{\mathrm{TS},i}}(i=1)$ of 1.77%, the error of the probability given by the GNN is only 0.09%. It indicates that the proposed GNN can accurately assess the probability for the index with a low probability. The results of $P_{R_{\mathrm{OS},i}}$ indicate that there is a multi-instability probability of 20.59% under the current operating condition, which is significantly larger than the probability of any type of singular instability. Hence, the proposed GNN can provide more comprehensive insights into potential risks compared with the SRA of singular stability.

The confusion matrices of different types of stability results are also given to demonstrate the assessment effects of the proposed method comprehensively, as shown in Fig. 5.

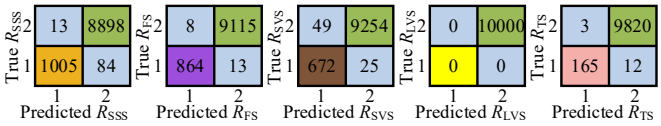

Fig. 5 Confusion matrices of different types of stability results in IEEE 39-bus system

According to the results in Fig. 5, the assessment results are biased to a certain degree from the perspective of misclassification numbers. However, from the perspective of misclassification rates, the proportion of biased results is quite low, which may hardly affect the accuracy of multi-stability risk results.

In order to further verify the superiority of the proposed GNN, the proposed GNN is compared with 5 widely employed machine learning methods, including decision tree (DT), support vector machine (SVM), artificial neural network

(ANN), CNN, and long-short-term memory (LSTM) network. The operating graph and disturbance graph are transformed into 1-dimensional vector features since the above method cannot process graph data. The assessment results of different machine learning methods are compared in TABLE IV.

TABLE IV
MAXIMUM ERRORS OF MULTI-STABILITY PROBABILITIES GIVEN BY DIFFERENT MACHINE LEARNING METHODS IN IEEE 39-BUS SYSTEM

Method	E_{SSS}	E_{FS}	E_{SVS}	E_{LVS}	E_{TS}	E_{OS}
Proposed GNN	**0.71%**	**0.05%**	**0.24%**	**0%**	**0.09%**	**0.65%**
DT	5.64%	0.30%	1.75%	0%	0.58%	6.03%
SVM	2.93%	3.62%	2.90%	0%	0.92%	6.88%
ANN	4.78%	5.94%	4.00%	0%	0.97%	8.14%
CNN	2.51%	0.20%	0.44%	0%	0.15%	2.92%
LSTM	1.80%	0.07%	0.59%	0%	0.46%	1.40%

In TABLE IV, taking the results given by the eigenvalue analysis and TDS as a benchmark, E_{SSS}, E_{FS}, E_{SVS}, E_{LVS}, E_{TS}, and E_{OS} are the maximum errors of the probabilities of small-signal, frequency, short-term and long-term voltage, transient, and overall stability, respectively, given by different methods. The DL methods (proposed GNN, CNN, and LSTM) demonstrate obviously low errors compared with the traditional DT, SVM, and ANN due to their strong fitting ability and generalizability. The lowest errors for all types of stability risks can be achieved by the proposed GNN since the spatial correlations in graph data can be well-mined.

3) SURs visualization results

By uniformly sampling for the active power of WF1, WF2, and WF3 (i.e., P_{WF1}, P_{WF2}, and P_{WF3}), 8000 potential scenarios are sampled to generate SURs. Considering different faults independently, corresponding naive SURs can be obtained and then be further aggregated as integrated SURs as follows.

Visualization of Naive SURs: Considering the occurrence of the three-phase-to-ground fault at line 8-9 under the 8000 potential scenarios, the corresponding naive SURs can be visualized by *Algorithm 1*, as shown in Fig. 6.

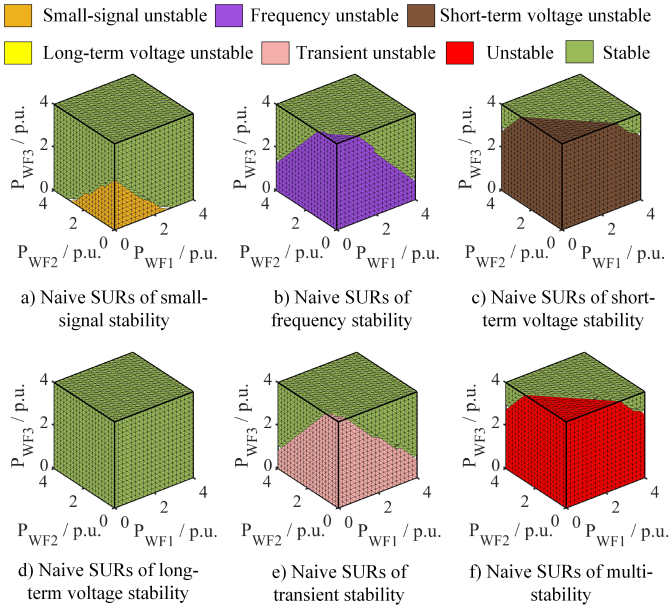

Fig. 6 Naive SURs of a fault at line 8-9 in IEEE 39-bus system

Fig. 6 shows that different types of stability have different SURs. In Fig. 6(a), the unstable region of small-signal stability is located near point (0, 0, 0). This is because the concerned oscillation mode is mainly associated with G10 (slack bus). The decrease in wind power generation results in an increase in the output of G10, thereby reducing the small-signal stability margin of the oscillation mode. The transmission power at line 8-9 increases when P_{WF1}, P_{WF2}, and P_{WF3} decrease, thereby causing transient instability and frequency instability when the fault occurs at line 8-9, as shown in Fig. 6(b) and Fig. 6(e). The increasing transmission power at line 8-9 and other critical lines reduces the steady-state voltages at buses 1, 2, 8, 9, etc., resulting in the short-term voltage instability after the fault at line 8-9, as shown in Fig. 6(c). By contrast, the system is always long-term voltage stable since the current operating point never exceeds the load limit regardless of the changes in P_{WF1}, P_{WF2}, and P_{WF3}, as shown in Fig. 6(d). The frequency, short-term voltage, and transient stability share a large unstable region, which indicates that the transient, short-term voltage, and frequency instability can occur simultaneously. The short-term voltage stability also has a partially unique unstable region, indicating singular short-term voltage instability in this region. Based on the naive SURs associated with overall stability in Fig. 6(f), the stable region that avoids multiple stability problems can be intuitively visualized for the reference by TSOs to mitigate the risk of multi-stability.

Visualization of Integrated SURs: According to the volume order of the unstable region, the naive SURs associated with overall stability considering different faults can be further aggregated into the integrated SURs associated with overall stability by *Algorithm 2*, as shown in Fig. 7.

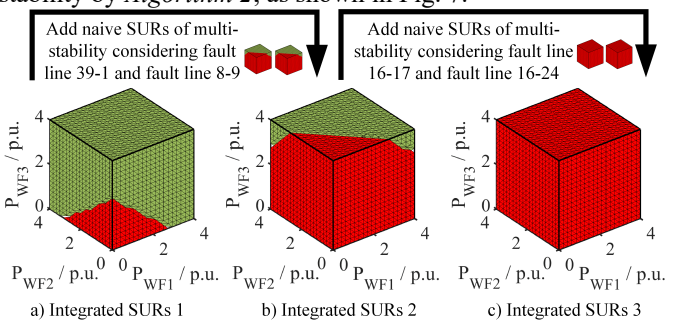

Fig. 7 Integrated SURs associated with overall stability in IEEE 39-bus system

In Fig. 7(a), the integrated SURs 1 are derived by integrating the naive SURs of 14 types of faults, including the trip of G1, G2, G3, G4, G5, and G7, and the faults at lines 2-3, 3-4, 3-18, 4-14, 6-11, 13-14, 26-27, and 26-28. The integrated SURs 1 have a large stable region, indicating that the multi-stability risk of the 14 types of faults can be easily avoided by operational control measures. For example, the output of some SGs can be improved to reduce the transmission power of the lines with heavy loads when the wind power generation drops to the unstable region. In Fig. 7(b), the naive SURs of the faults at lines 39-1 and 8-9 are added into the integrated SURs 1, resulting in the integrated SURs 2. The addition of the new SURs significantly enlarges the unstable region. TSOs can balance the cost of additional operational control measures and the additional multi-stability risk, thereby making acceptable decisions accordingly. In Fig. 7(c), the naive SURs of the faults at lines 16-17 and 16-24 are added into the integrated SURs 2,

resulting in the integrated SURs 3 filled with an unstable region. It indicates that the multi-stability risk of these two additional faults can hardly be avoided by operational control measures, and targeted emergency control measures should be made for them. It should be noted that this paper mainly focuses on MSRA rather than operational optimization. Hence, the specific operational control measures are not studied in detail.

4) Efficiency Analysis

In addition to the accuracy of assessment results, time consumption is crucial for real-time MSRA. The time to generate the features of sampled scenarios, assess probability of multi-stability, and visualize naive SURs is given in Fig. 8.

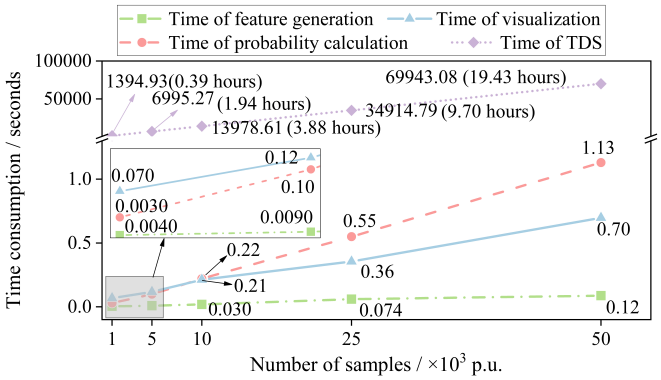

Fig. 8 Efficiency analysis in IEEE 39-bus system

The time consumption of each item in Fig. 8 increases linearly with the growth of the sample number. The features (i.e., operating graph and disturbance graph) of 10000 samples can be generated within 0.030 seconds since power flow calculation is avoided. Then, the multi-stability margin levels of the 10000 samples are assessed within 0.22 seconds by the proposed GNN, and the naive SURs are visualized within 0.21 seconds. Even considering 50000 samples, the whole process can be completed within 1.95 seconds. Hence, the proposed method has the potential for real-time MSRA and SURs visualization. By contrast, the eigenvalue analysis and TDS cost 3.88 hours for 10000 samples and 19.43 hours for 50000 samples. At least 99.94% of time consumption can be saved by the proposed method. It is noted that the time consumption is tested on a computer with a CPU of Intel i7-10700 and can be further reduced by using a high-performance server.

B. Test in A Modified WECC Power System

1) System description

A modified WECC 179-bus power system is employed to verify the effectiveness of the proposed MSRA method in a large-scale power system. The modified WECC power system has 29 SGs and 5 WFs. The information of an original WECC power system can be found in [46]. The 5 WFs (i.e., WF5, WF6, WF7, WF8, and WF9) are connected to buses 5, 60, 86, 161, and 174, respectively. The active power of WF5, WF6, and WF7 (i.e., P_{WF5}, P_{WF6}, and P_{WF7}) are regarded as the concerned uncertainties, as an example, to demonstrate the proposed method. The maximum active power of the three WFs is 5.0 p.u. A total of 14 transmission lines and 10 large capacity SGs are selected as the potential fault lines and fault SGs, respectively.

Considering the disturbance cases 1 and 2 at the system loading levels of 90%, 100%, and 110%, 27837 samples are generated as a training set to train the proposed GNN offline.

2) MSRA based on proposed GNN

As for the structure of the proposed GNN, the $\bar{M}^{(k)}$ of the FCL in each channel and the followed FCL are 8 and 256, respectively, and the maximum training epoch is 1000. The other hyperparameters of the proposed GNN are the same as those in the IEEE 39-bus system.

The proposed method is tested in the following operating conditions to verify the performance of online application. The actual system loading level is 91%, which is not included in the training set. By randomly sampling for the considered uncertainties above, 10000 test samples are generated for disturbance cases 1 and 2 based on the current operating condition. The probability of multi-stability given by the proposed GNN is given in TABLE V.

TABLE V
PROBABILITY OF MULTI-STABILITY GIVEN BY PROPOSED GNN IN WECC SYSTEM

Method	Margin level i	$P_{R_{\mathrm{SSS}},i}$	$P_{R_{\mathrm{FS}},i}$	$P_{R_{\mathrm{SVS}},i}$	$P_{R_{\mathrm{LVS}},i}$	$P_{R_{\mathrm{TS}},i}$	$P_{R_{\mathrm{OS}},i}$
Proposed GNN	2 (Stable)	100%	78.38%	82.25%	100%	97.47%	69.25%
	1 (Unstable)	0%	21.62%	17.75%	0%	2.53%	30.75%
Eigenvalue and TDS	2 (Stable)	100%	78.49%	82.00%	100%	97.30%	69.16%
	1 (Unstable)	0%	21.51%	18.00%	0%	2.70%	30.84%

In TABLE V, the maximum error in the predicted probability is 0.25%. For a low-probability case, i.e., $P_{R_{\mathrm{TS}},i}(i = 1)$ with 2.70%, the error is 0.17%. Hence, the proposed method can still provide the accurate probability of multi-stability in the modified WECC power system. Furthermore, the multi-instability probability (30.75%) is larger than the probability of any type of singular instability.

In addition, the confusion matrices are given in Fig. 9.

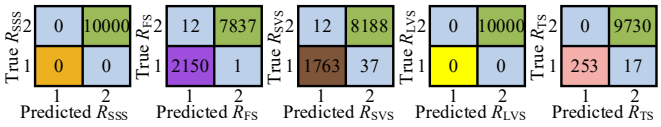

Fig. 9 Confusion matrices of different types of stability results in WECC system

According to the results in Fig. 9, a high accuracy (at least 99.51%) for each type of stability can be achieved by the proposed method in addition to the probability results.

3) SURs visualization results

Based on *Algorithms 1* and *2*, the naive SURs associated with overall stability considering different faults can be generated and then be aggregated as integrated SURs. The integrated SURs, including 14 types of faults, are always stable. It indicates no stability risks for these faults under the current operating condition. The integrated SURs that include the remaining types of faults are always unstable. Thus, instability can always be caused by these faults, and targeted emergency measures should be designed.

Furthermore, the dominant types of instability caused by the remaining faults can be analyzed by the proposed method. Based on the naive SURs associated with singular stability for the remaining faults, the dominant types of instability induced by each fault can be determined, as shown in Fig. 10.

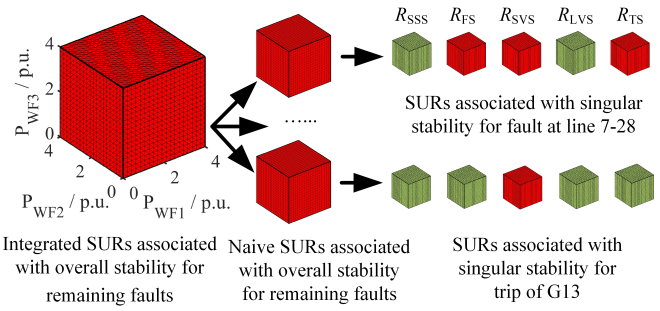

Fig. 10 Integrated SURs in WECC system

According to Fig. 10, the unstable region in the naive SURs for the fault at line 7-28 is generated due to frequency, short-term voltage, and transient instability. Similarly, the dominant types of instability induced by the other faults and corresponding locations are derived in Fig. 11 and TABLE VI.

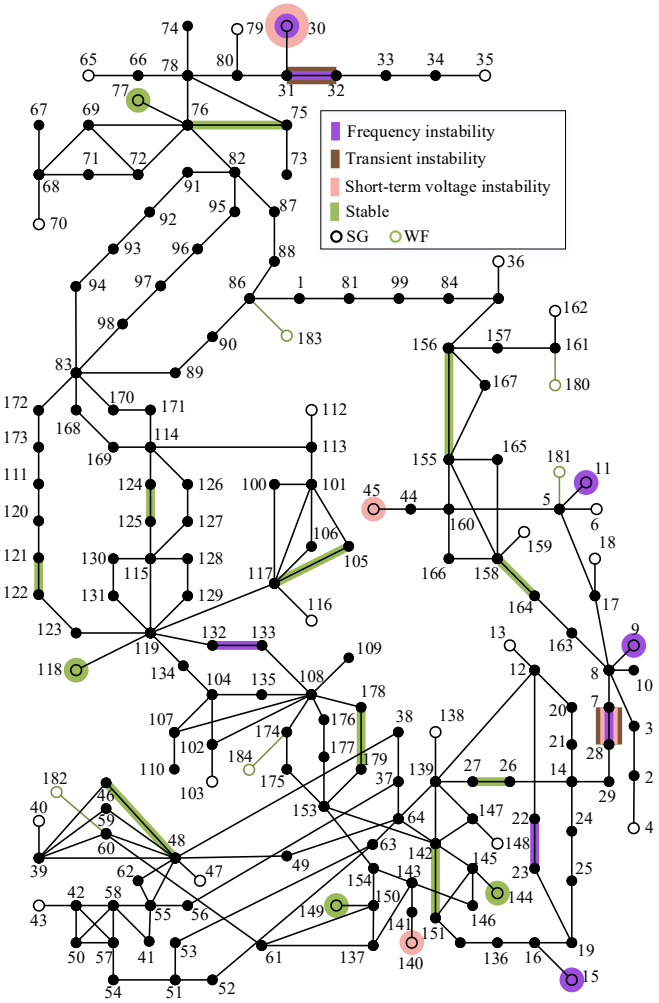

Fig. 11 Visualized dominant types of instability in WECC system

TABLE VI
DOMINANT TYPES OF INSTABILITY IN WECC SYSTEM

Instability type	Fault type
Small-signal	None.
Frequency	Trip of G3, G4, G6, and G8; Fault at lines 7-28, 22-23, 31-32, and 132-133.
Short-term voltage	Trip of G8, G13, and G24; Faults at lines 7-28.
Long-term voltage	None
Transient	Fault at lines 7-28 and 31-32.

In Fig. 11, dangerous fault locations can be understood intuitively. Then, according to TABLE VI, targeted measures can be designed according to the dominant types of instability to mitigate the risks of multi-stability effectively.

4) Efficiency Analysis

The time consumption of the proposed MSRA method in the modified WECC system is given in Fig. 12.

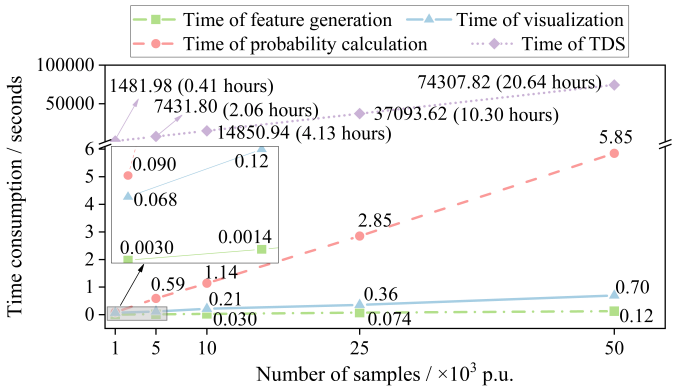

Fig. 12 Efficiency analysis in WECC system

The time consumption of each item in Fig. 12 grows linearly with the growth of the sample number. The proposed method can complete the MSRA based on 10000 samples within 1.65 seconds. Compared with eigenvalue analysis and TDS, at least 99.99% of time consumption is saved by the proposed method.

C. Test in A Modified GB Power System

In order to further verify the effectiveness of the proposed method in a large inter-connected system model, a case study in a modified GB system model is supplemented. The information of the GB system can be found in [47]. The modified GB system includes 2224 buses, 3207 branches, and 384 generators. Ten WFs are connected to the system as the uncertainty induced by renewable energy. The maximum active power of each WF is 5.0 p.u. Ten types of complex faults are considered as the representative uncertainty induced by faults, including 6 types of *N*-1 faults, 3 types of *N*-2 faults, and 1 type of *N*-3 fault. The occurrence probabilities of the faults are assumed in TABLE VII, which can be obtained correctly from historical data in practice.

TABLE VII
PROBABILITY OF FAULT OCCURRENCE IN GB SYSTEM

Fault (*N*-*k*)	Probability
Fault 1, 2, 3, 4, 5, and 6 (*N*-1)	12.00% for each
Fault 7, 8, and 9 (*N*-2)	8.00% for each
Fault 10 (*N*-3)	4.00%

At the system loading levels of 90%, 95%, 100%, 105%, and 110%, considering the uncertainty of faults and wind power generation, 30000 samples are generated as a training set to the proposed GNN offline.

The proposed method is tested in the following operating condition to verify the performance of the online application. The actual system loading level is 92%, which is not included in the training set. By randomly sampling for the considered uncertainties above, 5000 test samples of disturbance case 1 are generated based on the current operating condition. The probability of multi-stability given by the proposed GNN is shown in TABLE VIII.

TABLE VIII
PROBABILITY OF MULTI-STABILITY GIVEN BY PROPOSED GNN IN GB SYSTEM

Method	Margin level i	$P_{R_{\mathrm{SSS}},i}$	$P_{R_{\mathrm{FS}},i}$	$P_{R_{\mathrm{SVS}},i}$	$P_{R_{\mathrm{LVS}},i}$	$P_{R_{\mathrm{TS}},i}$	$P_{R_{\mathrm{OS}},i}$
Proposed GNN	2 (Stable)	100%	83.06%	85.88%	100%	87.34%	80.56
	1 (Unstable)	0%	16.94%	14.12%	0%	12.66%	19.44
Eigenvalue and TDS	2 (Stable)	100%	82.94%	85.70%	100%	87.12%	80.24
	1 (Unstable)	0%	17.06%	14.30%	0%	12.88%	19.76

In TABLE VIII, the probability values given by the proposed GNN are quite close to the values derived by eigenvalue analysis and TDS. The maximum error in the predicted probability is 0.32%, indicating the effectiveness of the proposed GNN in assessing the multi-stability risks induced by complex *N*-1, *N*-2, and *N*-3 faults in the modified GB power system.

V. CONCLUSION

In this paper, an MSRA method based on GNN is proposed to accurately determine the risks of multi-stability moment by moment, verified by the results given by eigenvalue analysis and TDS. At each moment, the MSRA can be completed by the proposed method within several seconds, thereby saving at least 99.94% of time consumption compared with eigenvalue analysis and TDS. The main findings are given below.

- The instability probability can be underrated by the SRA for singular stability as the instability probability and region of multi-stability can be much larger than those of any singular stability. By contrast, the stability risks can be assessed by the proposed method comprehensively and accurately. Compared with existing machine learning methods, the proposed method can achieve higher accuracy for MSRA.
- In general, the small-signal stability in large-scale power systems usually needs to be guaranteed before scheduling. Therefore, the stable operation region of long-term voltage stability and small-signal (converter-driven and small-disturbance rotor angle) stability are the largest and second largest, respectively, both of which are obviously larger than those of the other types of stability. As for the frequency, short-term voltage, and transient stability, the sizes and locations of their stable regions rely on specific faults and there is no absolute size relationship between them.
- The visualized SURs indicate that different types of instability can be induced independently or simultaneously by a fault when operating in different regions. Different faults lead to different dominant types of instability. Transient instability is mainly induced by faults at lines, and the frequency and short-term voltage instability can be induced by SG trip or faults at lines. Such results above can be given by the proposed MSRA method in detail instead of the SRA of singular stability.

Future work will focus on enhancing the interpretability of the MSRA based on GNNs, which is crucial to make the assessment results convincing. In addition, defending against the impacts of cyberattacks on the MSRA should be noticed.

REFERENCES

[1] R. Yan, N. Masood, T. Kumar Saha, F. Bai, and H. Gu, "The anatomy of the 2016 south Australia blackout: a catastrophic event in a high renewable network," *IEEE Trans. Power Syst.,* vol. 33, no.5, pp. 5374-5388, Sep. 2018.

[2] O. P. Veloza and F. Santamaria, "Analysis of major blackouts from 2003 to 2015: classification of incidents and review of main causes," *Electr. J.,* vol. 29, no.7, pp. 42-49, Sept. 2016.

[3] N. Verma, N. Kumar, S. Gupta, H. Malik, and F. P. García Márquez, "Review of sub-synchronous interaction in wind integrated power systems: classification, challenges, and mitigation techniques," *Prot. Control Mod. Power Syst.,* vol. 8, no.1, Apr. 2023.

[4] N. Hatziargyriou, J. Milanovic, C. Rahmann, V. Ajjarapu, C. Canizares, I. Erlich, D. Hill, I. Hiskens, I. Kamwa, B. Pal, P. Pourbeik, J. Sanchez-Gasca, A. Stankovic, T. Van Cutsem, V. Vittal, and C. Vournas, "Definition and classification of power system stability - revisited & extended," *IEEE Trans. Power Syst.,* vol. 36, no.4, pp. 3271-3281, Jul. 2021.

[5] K. N. Hasan, R. Preece, and J. V. Milanović, "Existing approaches and trends in uncertainty modelling and probabilistic stability analysis of power systems with renewable generation," *Renew. Sustain. Energy Rev.,* vol. 101, pp. 168-180, Mar. 2019.

[6] P. N. Papadopoulos and J. V. Milanovic, "Probabilistic framework for transient stability assessment of power systems with high penetration of renewable generation," *IEEE Trans. Power Syst.,* vol. 32, no.4, pp. 3078-3088, Jul. 2017.

[7] J. Wen, S. Bu, and F. Li, "Two-level ensemble methods for efficient assessment and region visualization of maximal frequency deviation risk," *IEEE Trans. Power Syst.,* vol. 38, no.1, pp. 643-655, Jan. 2023.

[8] Q. Chen, S. Bu, X. Zhang, S. Yi, and Y. Wei, "Spectral impedance-based probabilistic wideband oscillatory stability analysis and visualization," *IEEE Trans. Power Syst.,* pp. 1-13, 2024. (Early access) DOI: 10.1109/TPWRS.2024.3422173

[9] S. Bu, W. Du, and H. Wang, "Investigation on probabilistic small-signal stability of power systems as affected by offshore wind generation," *IEEE Trans. Power Syst.,* vol. 30, no.5, pp. 2479-2486, Sept. 2015.

[10] M. Fan, Z. Li, T. Ding, L. Huang, F. Dong, Z. Ren, and C. Liu, "Uncertainty evaluation algorithm in power system dynamic analysis with correlated renewable energy sources," *IEEE Trans. Power Syst.,* vol. 36, no.6, pp. 5602-5611, Nov. 2021.

[11] S. Bu, W. Du, H. Wang, Z. Chen, L. Xiao, and H. Li, "Probabilistic analysis of small-signal stability of large-scale power systems as affected by penetration of wind generation," *IEEE Trans. Power Syst.,* vol. 27, no.2, pp. 762-770, May 2012.

[12] K. N. Hasan, R. Preece, and J. V. Milanovic, "The influence of load on risk-based small-disturbance security profile of a power system," *IEEE Trans. Power Syst.,* vol. 33, no.1, pp. 557-566, Jan. 2018.

[13] H. Huang, C. Y. Chung, K. W. Chan, and H. Chen, "Quasi-monte carlo based probabilistic small signal stability analysis for power systems with plug-in electric vehicle and wind power integration," *IEEE Trans. Power Syst.,* vol. 28, no.3, pp. 3335-3343, Aug. 2013.

[14] S. Bu, W. Du, and H. Wang, "Probabilistic analysis of small-signal rotor angle/voltage stability of large-scale AC/DC power systems as affected by grid-connected offshore wind generation," *IEEE Trans. Power Syst.,* vol. 28, no.4, pp. 3712-3719, Nov. 2013.

[15] M. Wang and J. V. Milanovic, "Simultaneous assessment of multiple aspects of stability of power systems with renewable generation," *IEEE Trans. Power Syst.,* vol. 39, no.1, pp. 97-106, Jan. 2024.

[16] R. F. Mochamad, R. Preece, and K. N. Hasan, "Probabilistic multi-stability operational boundaries in power systems with high penetration of power electronics," *Int. J. Electr. Power Energy Syst.,* vol. 135, Feb. 2022.

[17] R. Preece, K. Huang, and J. V. Milanovic, "Probabilistic small-disturbance stability assessment of uncertain power systems using efficient estimation methods," *IEEE Trans. Power Syst.,* vol. 29, no.5, pp. 2509-2517, Sept. 2014.

[18] R. Preece and J. V. Milanovic, "Efficient estimation of the probability of small-disturbance instability of large uncertain power systems," *IEEE Trans. Power Syst.,* vol. 31, no.2, pp. 1063-1072, Mar. 2016.

[19] H. Marzooghi, M. Garmroodi, G. Verbic, A. S. Ahmadyar, R. Liu, and D. J. Hill, "Scenario and sensitivity based stability analysis of the high renewable future grid," *IEEE Trans. Power Syst.,* vol. 37, no.4, pp. 3238-3248, Jul. 2022.

[20] T. Su, Y. Liu, J. Zhao, and J. Liu, "Probabilistic stacked denoising autoencoder for power system transient stability prediction with wind farms," *IEEE Trans. Power Syst.,* vol. 36, no.4, pp. 3786-3789, Jul. 2021.

[21] B. Tan and J. Zhao, "Debiased uncertainty quantification approach for probabilistic transient stability assessment," *IEEE Trans. Power Syst.,* vol. 38, no.5, pp. 4954-4957, Sept. 2023.

[22] J. Wu and L. Li, "Power system frequency safety assessment scheme: multi-branch learning method based on ensemble full connection," *IEEE Trans. Power Syst.,* vol. 39, no.3, pp. 4805-4817, May 2024.
[23] Q. Chen, N. Lin, S. Bu, H. Wang, and B. Zhang, "Interpretable time-adaptive transient stability assessment based on dual-stage attention mechanism," *IEEE Trans. Power Syst.,* vol. 38, no.3, pp. 2776-2790, May 2023.
[24] Q. Chen, H. Wang, and N. Lin, "Imbalance correction method based on ratio of loss function values for transient stability assessment," *CSEE J. Power Energy Syst.,* pp. 1-12, 2022. (Early access) DOI: 10.17775/CSEEJPES.2021.00290
[25] R. Yan, G. Geng, Q. Jiang, and Y. Li, "Fast transient stability batch assessment using cascaded convolutional neural networks," *IEEE Trans. Power Syst.,* vol. 34, no.4, pp. 2802-2813, Jul. 2019.
[26] F. Shi, J. Wu, Y. Wang, L. Li, and Y. Zheng, "Integrated advance assessment of power system transient voltage and transient angle stability based on two-stage ensemble spatio-temporal graph neural network," *Measurement,* vol. 221, Nov. 2023.
[27] J. Huang, L. Guan, Y. Su, H. Yao, M. Guo, and Z. Zhong, "System-scale-free transient contingency screening scheme based on steady-state information: a pooling-ensemble multi-graph learning approach," *IEEE Trans. Power Syst.,* vol. 37, no.1, pp. 294-305, Jan. 2022.
[28] R. Zhang, W. Yao, Z. Shi, X. Ai, Y. Tang, and J. Wen, "Towards multi-scenario power system stability analysis: an unsupervised transfer learning method combining DGAT and data augmentation," *IEEE Trans. Power Syst.,* vol. 38, no.6, pp. 5367-5380, Nov. 2023.
[29] G. Lu and S. Bu, "Adaptive stability contingency screening for operational planning based on domain-adversarial graph neural network," *IEEE Trans. Power Syst.,* vol. 39, no.1, pp. 1503-1516, Jan. 2024.
[30] L. Chen and L. Guan, "Static information, k-neighbor, and self-attention aggregated scheme: a transient stability prediction model with enhanced interpretability," *Prot. Control Mod. Power Syst.,* vol. 8, no.1, Jan. 2023.
[31] X. Wu, W. Xu, and F. Xue, "Sample generation for security region boundary identification based on topological features of historical operation data," *J. Mod. Power Syst. Clean Energy,* vol. 12, no.4, pp. 1087-1095, Jul. 2024.
[32] Q. Chen, S. Bu, and C. Y. Chung, "Small-signal stability criteria in power electronics-dominated power systems: a comparative review," *J. Mod. Power Syst. Clean Energy,* vol. 12, no.4, pp. 1003-1018, Jul. 2024.
[33] T. Xu, A. B. Birchfield, and T. J. Overbye, "Modeling, tuning, and validating system dynamics in synthetic electric grids," *IEEE Trans. Power Syst.,* vol. 33, no.6, pp. 6501-6509, Nov. 2018.
[34] H. Wang, F. Gao, Q. Chen, S. Bu, and C. Lei, "Instability pattern-guided model updating method for data-driven transient stability assessment," *IEEE Trans. Power Syst.,* pp. 1-13, 2024. (Early access) DOI: 10.1109/TPWRS.2024.3429339
[35] L. Zhu, D. J. Hill, and C. Lu, "Hierarchical deep learning machine for power system online transient stability prediction," *IEEE Trans. Power Syst.,* vol. 35, no.3, pp. 2399-2411, May 2020.
[36] I. K. Bazionis, P. A. Karafotis, and P. S. Georgilakis, "A review of short-term wind power probabilistic forecasting and a taxonomy focused on input data," *IET Renew. Power Gener.,* vol. 16, no.1, pp. 77-91, Jan. 2022.
[37] M. Chen, Z. Wei, Z. Huang, B. Ding, and Y. Li, "Simple and deep graph convolutional networks," *in Proc. of the 38th ICML,* 2020.
[38] T. Cai, S. Luo, K. Xu, D. He, L. Tie-Yan, and L. Wang, "GraphNorm: a principled approach to accelerating graph neural network training," *in Proc. of the 38th ICML,* 2021.
[39] D. P. Kingma and J. L. Ba, "Adam: a method for stochastic optimization," *in Proc. of the 3rd ICLR,* 2015.
[40] H. Edelsbrunner, D. Kirkpatrick, and R. Seidel, "On the shape of a set of points in the plane," *IEEE Trans. Inf. Theory,* vol. 29, no.4, pp. 551-559, Jul. 1983.
[41] C. Ren, Y. Xu, B. Dai, and R. Zhang, "An integrated transfer learning method for power system dynamic security assessment of unlearned faults with missing data," *IEEE Trans. Power Syst.,* vol. 36, no.5, pp. 4856-4859, Sept. 2021.
[42] Z. Shi, W. Yao, Y. Tang, X. Ai, J. Wen, and S. Cheng, "Bidirectional active transfer learning for adaptive power system stability assessment and dominant instability mode identification," *IEEE Trans. Power Syst.,* vol. 38, no.6, pp. 5128-5142, Nov. 2023.
[43] C. Ren, H. Yu, Y. Xu, and Z. Y. Dong, "Understanding discrepancy of power system dynamic security assessment with unknown faults: a reliable transfer learning-based method," *CSEE J. Power Energy Syst.,* vol. 10, no.1, pp. 427-431, Jan. 2024.
[44] X. Li, Z. Yang, P. Guo, and J. Cheng, "An intelligent transient stability assessment framework with continual learning ability," *IEEE Trans. Ind. Inform.,* vol. 17, no.12, pp. 8131-8141, Dec. 2021.
[45] H. Cui, F. Li, and K. Tomsovic, "Hybrid symbolic-numeric framework for power system modeling and analysis," *IEEE Trans. Power Syst.,* vol. 36, no.2, pp. 1373-1384, Mar. 2021.
[46] S. Maslennikov, B. Wang, Q. Zhang, A. Ma, A. Luo, A. Sun, and E. Litvinov, "A test cases library for methods locating the sources of sustained oscillations," in *2016 IEEE PESGM*, 2016.
[47] "Power systems test case archive," Available: https://www.maths.ed.ac.uk/optenergy/NetworkData/fullGB/.

Qifan Chen received the B.Eng. and M.Eng. degrees in electrical engineering from Fuzhou University, Fuzhou, China, in 2018 and 2021, respectively. He was a visiting Ph.D. student at National University of Singapore, Singapore. He is currently working toward the Ph.D. degree with the Department of Electrical and Electronic Engineering, The Hong Kong Polytechnic University, Kowloon, Hong Kong. His research interests include power system transient stability and small signal stability analysis, and the application of machine learning in power system stability.

Siqi Bu (S'11-M'12-SM'17) received the Ph.D. degree from the electric power and energy research cluster, The Queen's University of Belfast, Belfast, U.K., where he continued his postdoctoral research work before entering industry. Then he was with National Grid UK as an experienced UK National Transmission System Planner and Operator. He is an Associate Professor and Associate Head with Department of Electrical and Electronic Engineering, The Hong Kong Polytechnic University, Kowloon, Hong Kong, and Associate Director of Research Centre for Grid Modernisation. He is also a Chartered Engineer with UK Royal Engineering Council, London, U.K. and a Fellow of IET. His research interests include power system stability, operation and economics considering renewable energy integration, smart grid application and transport electrification.

Dr. Bu is an Editor of *IEEE Transactions on Power Systems*, *IEEE Transactions on Consumer Electronics*, *IEEE Open Access Journal of Power and Energy*, *CSEE Journal of Power and Energy Systems*, *Protection and Control of Modern Power Systems*, *Journal of Modern Power Systems and Clean Energy* and *Advances in Applied Energy*.

Huaiyuan Wang received the B.Eng. and Ph.D. degrees in electrical engineering from Xi'an Jiaotong University, China, in 2010 and 2016. Currently, he is an Associate Professor with the College of Electrical Engineering and Automation, Fuzhou University, China. His research interests are power systems modeling, protection and control.

Chao Lei (Member, IEEE) received the Ph.D. degree in Electrical Engineering from The Hong Kong Polytechnic

University, Hong Kong. Previously, he was a visiting PhD student at National University of Singapore, Singapore. He is currently a Postdoctoral Research Fellow with the Department of Electrical and Computer Engineering, The University of British Columbia, Vancouver, BC, Canada. His research focuses centers around power system optimization and AI, high-fidelity battery simulation, and cyber-physical system security and privacy protection.